Journal of Biomechanics 91 (2019) 51–60

Contents lists available at ScienceDirect

Journal of Biomechanics

journal homepage: www.elsevier.com/locate/jbiomech
www.JBiomech.com

Implementation of controlling strategy in a biomechanical lower limb model with active muscles for coupling multibody dynamics and finite element analysis

Fuhao Mo [a,b], Junjie Li [a], Minchao Dan [a], Tang Liu [c,*], Michel Behr [b]

[a] State Key Laboratory of Advanced Design and Manufacture for Vehicle Body, Hunan University, Changsha, Hunan 410082, China
[b] Aix-Marseille University, IFSTTAR, LBA UMRT24, Faculté de Médecine Nord, Boulevard Pierre Dramard, 13916 Marseille Cedex 20, France
[c] Department of Orthopedics, The Second Xiangya Hospital of Central South University, 139 Renmin Road, Changsha, Hunan 410011, China

ARTICLE INFO

Article history:
Accepted 4 May 2019

Keywords:
Lower limb
PID control
CMC control
Muscle activation
Finite element analysis

ABSTRACT

Computational biomechanics for human body modeling has generally been categorized into two separated domains: finite element analysis and multibody dynamics. Combining the advantages of both domains is necessary when tissue stress and physical body motion are both of interest. However, the method for this topic is still in exploration. The aim of this study is to implement unique controlling strategies in finite element model for simultaneously simulating musculoskeletal body dynamics and in vivo stress inside human tissues. A finite element lower limb model with 3D active muscles was selected for the implementation of controlling strategies, which was further validated against in-vivo human motion experiments. A unique feedback control strategy that couples together a basic Proportion-Integration-Differentiation (PID) controller and generic active signals from Computed Muscle Control (CMC) method of the musculoskeletal model or normalized EMG singles was proposed and applied in the present model. The results show that the new proposed controlling strategy show a good correlation with experimental test data of the normal gait considering joint kinematics, while stress distribution of local lower limb tissue can be also detected in real-time with lower limb motion. In summary, the present work is the first step for the application of active controlling strategy in the finite element model for concurrent simulation of both body dynamics and tissue stress. In the future, the present method can be further developed to apply it in various fields for human biomechanical analysis to monitor local stress and strain distribution by simultaneously simulating human locomotion.

1. Introduction

Human body models (HBMs) are widely used for biomechanical analysis in biomedical engineering, transport safety, sport science, and other human involved activities (Florio, 2018; Halloran et al., 2010; Hedenstierna and Brolin, 2008; Lenhart et al., 2015). Compared with experimental tests, HBMs have higher flexibility and a wider range of application regarding ethics and loading conditions. Till now, HBMs primarily include multi-rigid body models (or musculoskeletal models) and finite element models (Dibb et al., 2013; Halloran and Erdemir, 2011). The multi-rigid body model is primarily composed of many rigid bodies connected by 1D muscle and joint hinges, and it can be used to simulate human kinematics during various loading conditions. The finite element model is more detailed and can provide local stress and strain information for inner tissues. However, it is not easy to simulate body kinematics with active locomotion. Therefore, combing the advantages of these two methods can facilitate stress and strain prediction in local tissue under physical loading conditions of human body motion (Phillips et al., 2015; Stops et al., 2012).

To achieve this purpose, most previous studies extracted loading conditions and muscle activation forces from musculoskeletal models, and then they applied them to finite element (FE) models to analyze the stress or strain responses of local tissues during different phases of human movement (Chen et al., 2015; Chen et al., 2010; Guiotto et al., 2014; Scarton et al., 2018; Zhihui et al., 2013). For example, Scarton et al. (2018) and Chen et al. (2015) extracted muscle forces and action lines through musculoskeletal gait analysis, and applied them on FE foot model for exploring plantar pressure of the diabetic foot. But this method is generally using quasi-static analysis by considering several specific phases

* Corresponding author.
E-mail address: liutang1204@csu.edu.cn (T. Liu).

https://doi.org/10.1016/j.jbiomech.2019.05.001
0021-9290/

of a gait cycle. Recently, some researchers implanted articular surface contact theories into the musculoskeletal models to obtain the joint contact force and stress in detail (Lenhart et al., 2015; Lin et al., 2010; Thelen et al., 2014). For example, Lin et al. (2010) and Thelen et al. (2014) coupled musculoskeletal model and joint contact model to predict local loading and stress variation in the knee joint during the entire gait. But this method is limited concerning the contact model and the theory of the multibody kinematics.

Direct active FE muscle modeling was also implemented in several human body or segment models (Budziszewski et al., 2008; Chang et al., 2008; Hedenstierna and Brolin, 2008; Osth et al., 2012; Iwamoto et al., 2009; Iwamoto et al., 2012; Iwamoto et al., 2011). Generally, 1D element with Hill law was used in these models (Budziszewski et al., 2008; Chang et al., 2008; Osth et al., 2012). Some models presented novel modeling methods with 3D geometry (Hedenstierna and Brolin, 2008; Iwamoto et al., 2009; Iwamoto et al., 2012; Iwamoto et al., 2011). Furthermore, several recent studies directly integrated muscle controlling strategy in FE human models. These models can be divided into two categories. The first type is using the open-loop control methods, which pre-defined the muscle activation levels before simulation analysis (Iwamoto et al., 2009; Iwamoto et al., 2012). The second type is using the closed-loop control method (Osth et al., 2012; Osth et al., 2014), in which the muscle activation levels were defined based on real-time feedback of the virtual sensor in the FE model. Referring to the open-loop control, some studies have preset the muscle activation levels in FE models based on normalized muscle surface electromyography (EMG) signals to characterize the influences of active muscle forces on stress or strain distributions of local tissues (Behr et al., 2006; Behr et al., 2010; Chang et al., 2009; Jonkers et al., 2003; Mo et al., 2018). With the closed-loop controlling strategy, several recent studies reported the basic proportion integration differentiation (PID) control method on 1D active muscle FE models to stimulate posture maintenance of drivers during vehicle impacts (Osth et al., 2012; Osth et al., 2014). Most recently, Salin et al. (2016) from IFSTTAR Institute, established a closed-loop controlling technique to simulate muscle reflex loop, and they applied it to an FE arm model containing active muscles for weight lift simulation.

The present study aims to seek a unique method to combining multibody dynamic analysis and finite element analysis by implementing a novel muscle controlling strategy in a FE human body model. Based on a lower limb model with 3D active muscles, a novel feedback controlling strategy was proposed by combining pre-defined activation levels with a PID control method. The availability and advantage of this new proposed control strategy and combined analysis method were discussed in consideration of joint kinematics and muscle activation.

2. Methods and materials

2.1. Introduction of combined muscle controlling strategy

Details support the finite element lower limb model with 3D muscles used in the present study have been introduced in the Appendix. The abbreviations are listed in Table A3. As shown in Fig. 1, a novel feedback control strategy for the present model was developed including pre-defined activation levels from the CMC controller of the musculoskeletal model and a PID controller implanted in the FE model. The CMC control method was used to compliment generic muscle activation levels to drive the FE model, while the PID controller was primarily used to iteratively adjust muscle activation at each time step during the gait analysis.

$D(t)$ was the target joint angle from the experimental results (Barrett et al., 2007). The initial activation levels of $A(t)$ were acquired from the CMC controller of a general musculoskeletal model (Gait2392_Simbody) (Arnold and Martell, 2010) to drive the lower limb FE model and obtain the knee joint angle. Then, the simulated knee joint angle $y(t)$ then compared with $D(t)$ to get an error signal $e(t)$, namely, the difference between the feedback signal y(t) and the target joint angle $D(t)$. In the following step, a neural delay module was employed to simulate the neural delay mechanism of central nervous system. Sequent, the PID controller regulated the delayed error signal and obtained the muscle excitation signal $u(t)$. Then, this muscle excitation signal was transferred to a muscle activation level $A(t)$ with two low-pass filters based muscle activation dynamics. Finally, the initial muscle activation levels were updated and iteratively updated at each time step to minimize the error signal $e(t)$.

The details of the knee joint angle calculation, PID and CMC control algorithm, neural delay simulation and muscle activation dynamics are described in the Appendix.

2.2. Comparison of different muscle controlling methods

To verify the availability and accuracy of the control strategy, the present muscle control method was integrated into the lower limb FE model with 3D active muscles for simulation analysis. Based on the experimental data (Arnold et al., 2013; Barrett et al., 2007) of the volunteers, gait analysis using the present method was compared with other controlling methods. All controlling methods investigated were categorized into three groups as follows.

(1) Pre-defined activation levels based on EMG signals or CMC controller

Muscle activation levels during the swing phase of the gait were investigated with volunteer experiments. The normalized muscle activation levels of nine lower limb superficial muscles were acquired with a nonlinear discrete recursive equation based on full-wave rectified, and low-pass filtered EMG data (Arnell, 1988), while the curves were also phase-shifted by 20 ms to account for electromechanical delays between the stimulation of the muscles and corresponding excitation. As generally implemented by the open-loop control, the muscle activation levels of all 9 muscles obtained from (Barrett et al., 2007) experiments were set as input signals for the 3D muscles of the present lower limb FE model. Some typical muscle activation levels are shown in Fig. 2. The muscle activation levels from EMG experiments were calculated as follows:

$$E_{RMS} = \left[\frac{1}{T}\int_{t}^{t+T} EMG^2(t)dt\right]^{1/2} \quad (1)$$

$$A(t) = E_{RMS}/E_{RMS\max} \quad (2)$$

where E_{RMS} is the root mean square value of EMG signal, and T is the sampling period. In the following result part, this method corresponds to Case A.

In addition, the same nine muscle activation levels calculated by the solo CMC controller of the musculoskeletal model were also obtained for the gait analysis. Typical activation levels were also listed in Fig. 2. The results were compared with application of the EMG signals. As in the aforementioned method, the validated musculoskeletal model (Gait2392_Simbody Opensim 3.3) in Opensim codes was used for gait analysis (Arnold and Martell, 2010). The CMC control method was used to calculate generic muscle activation levels. The initial muscle activation levels calculated

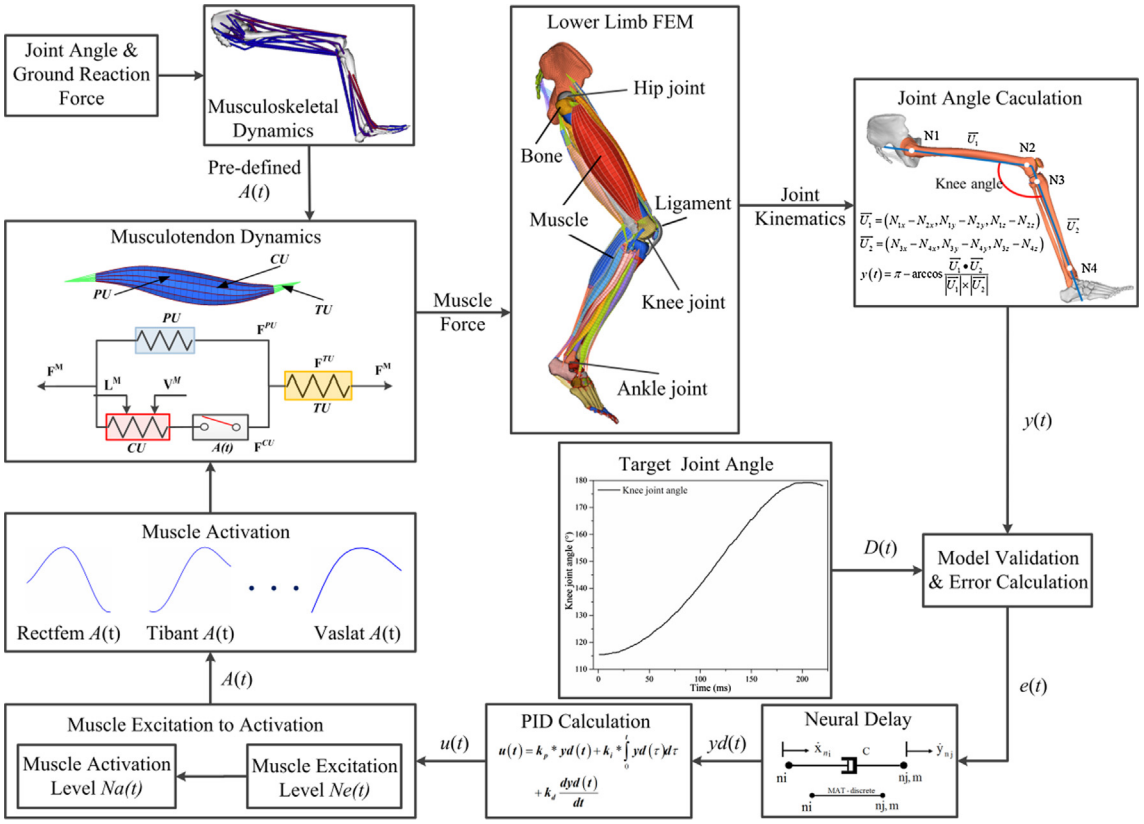

Fig. 1. Schematic of combined muscle control strategy.

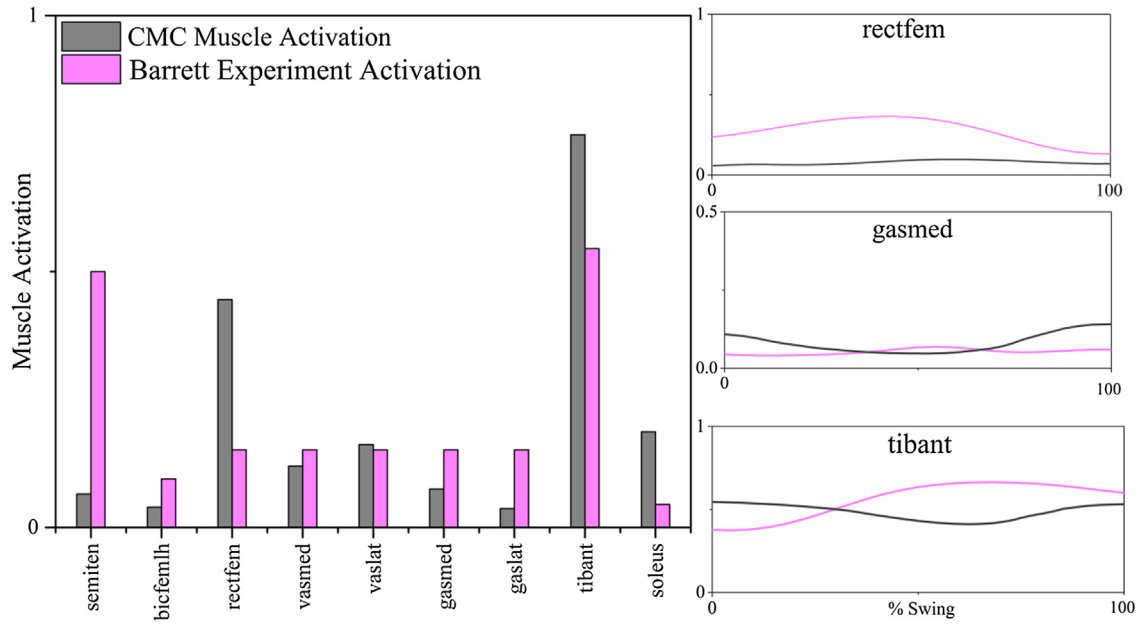

Fig. 2. Pre-defined lower limb superficial muscles activation levels of the CMC method and experimental EMG signals for the FE lower limb model (Barrett et al., 2007).

by the solo CMC controller of the musculoskeletal model were also obtained for the gait analysis. In the following result part, this method corresponds to Case B. As shown in Fig. 2, it is noted that activation levels calculated from the CMC controller present significant difference with the experimental results (Barrett et al., 2007). Even the experimental results with the similar gait speed present evident difference concerning normalized EMG signals.

(2) Sole PID control based on knee joint kinematics

In this control method, the knee joint angle curve of the volunteer was extracted as the target value for the PID controller, as shown in the target joint angle of Fig. 1 (Barrett et al., 2007). The lower limb FE model was placed in a gravitational field with an acceleration of 9.81 m/s^2. The pelvis part of the model was

constrained in translational and rotational freedoms: X, Y, and Z directions. The simulation was carried out until 220 ms as indicated by the experiments, which included the gait phase from the maximum flexion of the lower limb to full extension. The knee joint angle curve was set as input signals. The PID controller was used to calculate the control signal $u(t)$, which was then transferred to the muscle activation levels $A(t)$. Finally, the FE lower limb were driven by these automatic generated $A(t)$s to adjust the knee joint angle to minimized the error signal, and match the inputted knee joint angle. In the following result part, this method corresponds to Case C.

(3) Combination of pre-defined activation levels and PID controller

This method was as a combination of the pre-defined activation levels and a PID controller. As shown in Fig. 2, the initial activation levels of lower limb superficial muscles were pre-defined by the results of Case A and Case B, respectively. These initial inputs for the lower limb FE model were combined with the PID feedback control method to perform gait analysis. This method drove the lower limb FE model with activation of the 3D muscles, and it limited errors with the target motion states by monitoring the real-time output of the knee joint angle. The PID controller continuously updated muscle activation levels for continuous lower limb motion; this method corresponds to Case D and Case E.

3. Results

Lower limb kinematics with different muscle controlling strategies was compared with experimental test results as shown in Fig. 3. Each swing phase simulation was performed over a 220 ms duration using the LS-DYNA solver with the time step size of 0.00027 ms. The correlations of knee joint angles with time are shown in Fig. 3. The results of Case A and B represent the open-loop control strategy with the pre-defined activation levels, which were based on normalized EMG signals and the activation levels of the CMC control, respectively. In Case A, The simulation results differed greatly from the experimental results, with a coefficient of determination R_A^2 equaled to 0.32, and a root mean square error $RMSE_A$ equaled to 13.6°. Case B represents the open-loop control strategy with activation levels generated by CMC control. R_B^2 equaled to 0.86, and $RMSE_B$ was 6.19°.

Case C indicates the results with the solo PID control strategy for knee joint kinematics. The calculated R_C^2 and $RMSE_C$ are 0.69 and 9.75°, respectively Case D and Case E indicate the results from the control methods of combining the pre-defined generic activation levels and the PID controller. The PID controller combined with EMG-based pre-defined levels corresponds to Case D, while the PID controller with CMC-based pre-defined levels corresponds to Case E. The simulation result of Case D presents a good agreement with the experimental test data. The calculated R_D^2 is 0.63, and the $RMSE_D$ is approximately 10.61°. Although with the similar method, Case E reports large difference with the experimental results by R_E^2 equaling to 0.98 and $RMSE_E$ equaling to 3.03°.

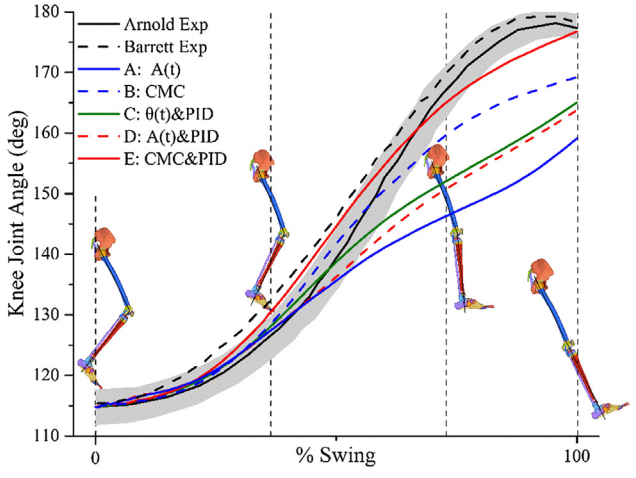

Fig. 3. Comparison of simulation results of different control strategies with experimental results. Data represent the mean (black line) ± 1 SD (shaded region).

The normalized active muscle levels generated by the coupling CMC and PID controlling method were shown in Fig. 4. Compared with the pre-defined muscle activation levels by the CMC control method of the musculoskeletal model, the muscle activation levels were significantly adjusted. Specifically, the activation amplitudes of biceps femoris long head, vastus medialis, vastus lateralis and gastrocnemius lateralis were obviously increased, while those of other muscles were significantly reduced. The quadriceps and tibialis anterior activation levels were much bigger than others, as they played a primary role during the swing gait. The two experimental test results also show some difference considering muscle activation levels under similar gait speed of 1.25 m/s and 1.30 m/s, especially considering semitendinosus and rectus femoris. The adjusted muscle activation levels through the present controlling strategy show a close tendency to the experimental results of Barrett et al. (2007) excluding the muscle semitendinosus and rectus femoris regardless of the amplitude and shape of the muscle activation curves.

In addition, the motions states and contact pressures at the knee and ankle joints of the lower limb model during the entire swing phase are presented in Fig. 5. In the simulation animation, the activation levels of quadriceps and tibia anterior muscles were obviously higher than the others. During this stage of the gait cycle, the maximum pressure of the femur articular cartilage and tibia plateau cartilage is about 1.5 MPa, and 6.57 MPa at the talus cartilage.

4. Discussion

As numerical modeling of the human body has been developed, the simulation of active muscle effects in the finite element model has become an efficient way to consider realistic boundaries or loading conditions for corresponding biomechanical analyses. Compared with musculoskeletal model, the 3D FE model can better consider the effects of muscle fiber angles, muscle geometry, and tendons on muscle force. In previous studies, the most common way to achieve tissue stress analysis considering gait cycle loading is by combining dynamic analysis of a musculoskeletal model and FE analysis of a body segment model (Chen et al., 2015; Chen et al., 2012; Guiotto et al., 2014; Scarton et al., 2018; Zhihui et al., 2013). Generally, the muscle forces at specific phases of the gait cycle were extracted through the musculoskeletal model analysis and applied to the FE model for quasi-static analysis under these specific phases, like stance loading of (Guiotto et al., 2014; Scarton et al., 2018) gait cycle, push-off phase of (Chen et al., 2015; Chen et al., 2012; Zhihui et al., 2013) gait cycle, etc. With this type of loading methods, only tissue stress at specific several steps can be noted. In addition, the FE model structures considering specific status and boundary conditions should be adjusted and sometimes postulated to fit physical status of a lower limb during a gait cycle. This would also largely limit the prediction accuracy of the FE model. Research on how to apply muscle excitation properly in FE models has just begun; most of previous studies were primarily focused on the domain of driver's responses to car crash situation (Budziszewski et al., 2008; Chang et al., 2008; Hedenstierna and Brolin, 2008;

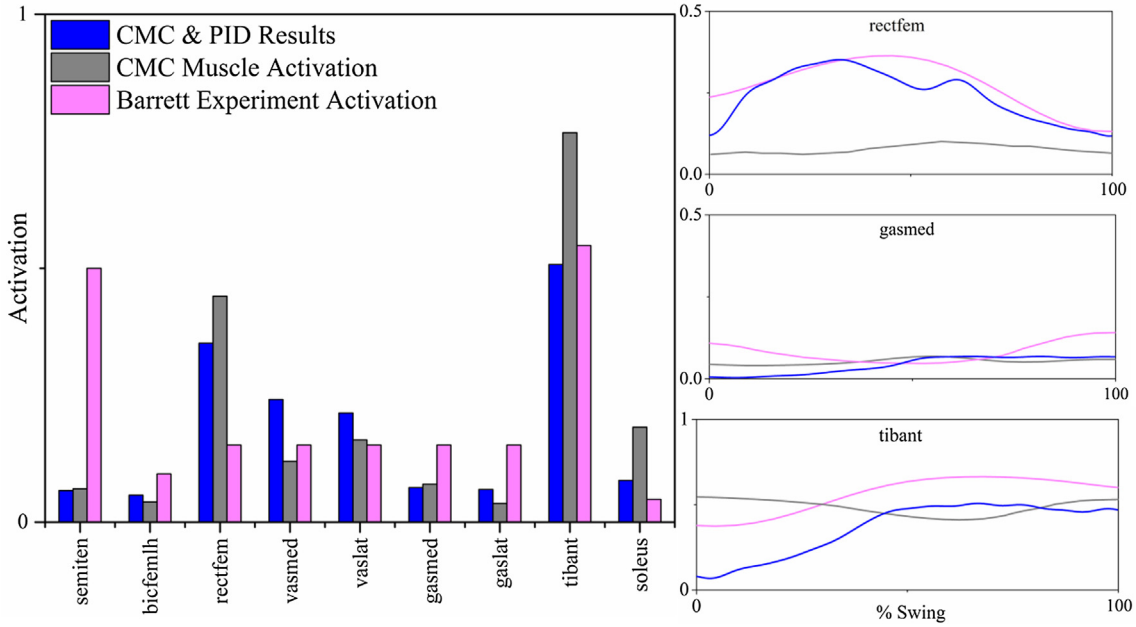

Fig. 4. Muscle activations comparison of experimental results with simulation results.

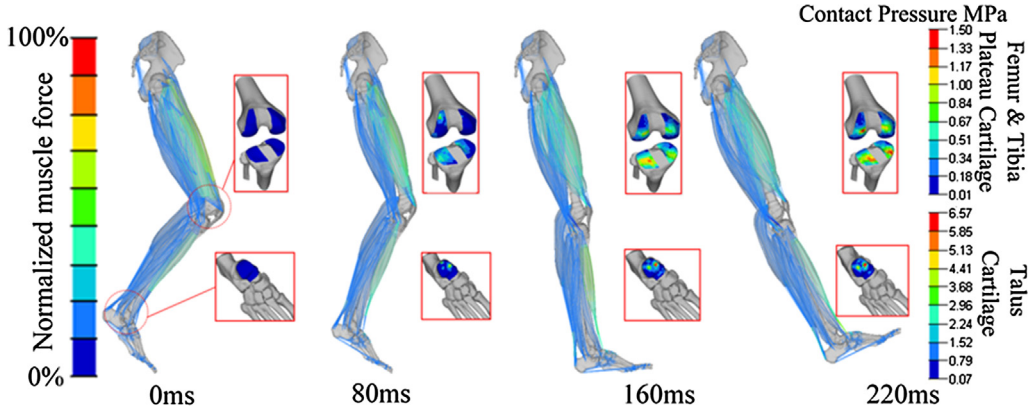

Fig. 5. Comparison of motion states and contact pressure distributions at the knee joint and ankle joint during the entire swing phase.

Iwamoto et al., 2012; Iwamoto et al., 2011; Scarton et al., 2018). The present study tried to implement muscle controlling strategies in a FE lower limb model to achieve dynamic gait analysis. By this method, we can detect continuous s tissue stress variation during the gait cycle as shown in Fig. 5. This also indicates that in future study we can detect dynamic index related to tissue stress or pressure responses, like center of pressure trajectory (COP) of the foot, etc.

The present study proposed a combined muscle control strategy, which was compared with several other strategies, and we evaluated the availability and efficiency of this strategy using a lower limb model with 3D muscles for a general human gait simulation. As the results showed, the open-loop control with predefined activation levels translated from EMG signals was limited, as a large gap between the simulations and experimental was observed. This large difference was due to limits when monitoring surface EMG signals. The EMG signals of deep muscles cannot be properly detected; therefore, these signals cannot fully reflect the excitation of human muscles (Mo et al., 2017). In addition, the simple translation from volunteer test data to a general human body model can be another limit, and because different human bodies have various muscle properties, even they have very similar statures. When only the PID controller was employed, the difference between the results of the experimental test and simulation was still significant. However, for simple posture maintenance, the simulation can be sufficient, as indicated by the previous studies (Bose and Crandall, 2008; Brown and Shaw, 1985). In a case of complex forward motion, the accuracy of simulated kinematics dynamics can be limited.

We next combined pre-defined activation levels from EMG signals or from the CMC control method, using a general musculoskeletal model with the PID controller, to calculate muscle excitation. Combining the generic activation levels from the CMC method with the PID controller generated the best correlation with the experimental data. The muscle activation levels were also adjusted more close to the EMG signals recorded in the experiments as shown in Fig. 4. Thus, it can indicate an important advantage of this muscle control strategy is that we can simulate human motion with the finite element model using pre-defined muscle activation levels from a musculoskeletal model instead of measuring EMG signals from specific individuals. Besides, the sensitivity analysis of PID parameters' effects on the lower limb kinematics

was initially investigated through scaling the k_p and k_d values to 0.1 and 10 times. The fixed PID parameters during the present lower limb locomotion present no significant influences on the results. The influence of neural delay time was also investigated. Although neural delay can be physical meaningful, our present model showed ignorable difference considering different neural delay setting from 0 ms to 50 ms.

The contact pressure at the knee joint and ankle joint were recorded during the lower limb swing, as shown in Fig. 5. Few previous studies show this type of contact distribution (Brown and Shaw, 1985; Fukubayashi and Kurosawa, 1980; Sangbaek et al., 2019; Shirazi et al., 2008), due to difficulties of in-vivo experiments and dynamic simulations. A peak contact pressure of 1.6 to 3.2 MPa was considered to be reasonable for the whole gait stage. The present study only simulated a swing phase of the gait cycle, the smaller peak value of 1.5 MPa were noted in the knee joint and can be reasonable compared to the previous studies (Brown and Shaw, 1985; Fukubayashi and Kurosawa, 1980; Sangbaek et al., 2019; Shirazi et al., 2008). However, the high pressure value of 6.57 MPa in the ankle joint was noted. This can be due to the limits of some leg muscle modeling, which involve in the foot motion. As the present study was primarily focused on knee joint motion, some foot motion related muscles were not fully passing through to the forefoot due to its complicated connecting pathway and uncertain tendon properties, such as peroneal longus, peroneal brevis and tibialis posterior. These muscles insertions end around the ankle joint, while the gastrocnemius is still connected to the calcaneus by the tendon. All these can result in excessive stress around the ankle joint. Thus, it is necessary to further improve the lower limb model for a whole gait analysis in the future.

The present study is an initial attempt to implement PID control in a 3D muscle FE model. Although it is a good choice for detecting tissue stress with dynamic motion loading, there are still some drawbacks. First, neural network or other complicated controlling strategies can be also combined with PID control for automatically obtaining PID gains in the future. However, as noticed in Salin et al. (2016) study, our study also found that integrating muscle controlling strategy in the FE model would significantly increase the model calculation time. The computational cost is much higher than motion simulation with a musculoskeletal model. The current case with the solo PID controller takes approximately 22 h in an 8-CPU working station (Intel (R) xeon (R) CPU E5-1620 v2 @ 3.70 GHz). A balance between controlling method and research purposes should be achieved for application consideration.

Second, due to the complexity of model contact setting, the stability and controlling strategy of the FE model still requires improvement. In the present study, only swing phase of normal walking gait was simulated due to the aforementioned limits. For other phases of foot interaction with grounds, moving hip joint kinetics needs to be added, where a balance control program can be necessary. All these can largely increase calculation cost and instability for the model, and limit the model application. Regarding rapid development of computation, it is still one improving direction for the model. On the other hand, one solution can be that combining the current model with dynamic loading condition modeling for foot-ground interaction.

Third, the present FE model represents a typical 50th percentile male for these simulations, which was not personalized according to volunteer data. To established a subject-specific lower limb model, a numerical tool with geometry scaling and personalized parameter setting as presented in the previous studies can be helpful (Valente et al., 2017; Wang et al., 2016). Muscle properties can be personalized based on MRI images or experimental tests. The personalized method of the FE lower limb model should be explored and used to further validate the present controlling strategy.

5. Conclusion

This study presents the development of a novel muscle control strategy in an FE lower limb model with 3D muscles, and then it was compared with other muscle control strategies through general human gait simulation. The proposed control methods for muscle activation combined pre-defined activation levels and the PID controller, showing good prediction for human kinematics, especially when the PID controller was coupled with generic activation levels extracted from the CMC method of a musculoskeletal model. This method also indicates that pre-defined muscle activation levels generated by the CMC method can be coupled with the PID controller for FE lower limb model locomotion, which avoids complex experimental measurements of EMG signals for driving the FE model. In addition, combining a muscle controller with an FE model enabled prediction of tissue stress and strain during the entire movement. This can be an alternative and reasonable choice for accurate biomechanical analysis when dynamic boundary conditions and active muscle forces have to be considered.

Declaration of Competing Interest

The authors declared that they have no competing interests about this study.

Acknowledgments

This study was supported by National Natural Science Foundation of China (Grant No. 51875187, 51621004), and Hunan Province Science and Technology Plan (2019JJ40021). The authors thank Opensim for providing support to obtain muscle activation levels.

Appendix

A 1. Details support the finite element lower limb model with 3D muscles

A 1.1. Lower limb model with 3D controllable muscles

The finite element lower limb model used in the present study is primarily based on CT and MRI images from a male close to the 50th percentile (weight 69.7 kg, height 173.1 cm). The lower limb model contains 11 thigh muscles and 11 shank muscles, which are simulated with detailed 3D geometries and controllable activation elements (Fig. A1). The whole model consists of 177,924 elements, of which there are 121,006 solid elements, 43,767 shell elements, 11,897 active contraction truss elements and 558 spring elements. The FE model was developed in LS-DYNA codes. Mimics and Geomagic were used to exact and separate the tissue geometry, and then ANSYS ICEM CFD and HyperMesh were used to map the hexahedral elements and define other element. In particular, the muscles were represented by a combination of 3D hexagonal elements and surrounding 1D truss elements, in order to simulate muscle contraction with detailed anatomy structures in parallel to consider their passive deformation.

The contacts between muscles and bones were defined as automatic surface to surface, and the contacts between meniscus and the tibial plateau cartilage was defined as tide nodes to surface. For some regions, additional adipose tissues were primarily filled between the muscles with sharing nodes on muscle surfaces or with 1D tension only elements. For some uncovered regions, muscle interactions were defined with automatic surface to surface contacts. Some details related to modeling method and material properties supporting the present model have been reported in

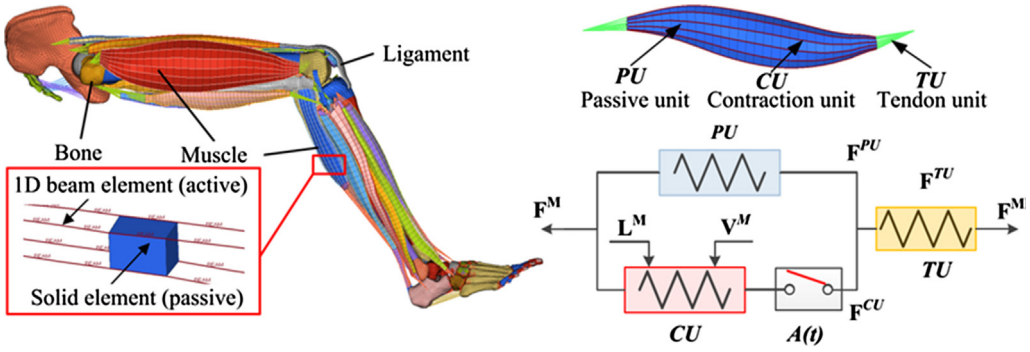

Fig. A1. Lower limb-pelvis FE model with 3D active muscles (F^M is the total muscle force, F^{CU} is the active muscle force, F^{PU} is the passive muscle force, F^{TU} is the tendon force; L^M is the normalized muscle fiber length curve, V^M is the normalized muscle fiber velocity curve, $A(t)$ is the muscle activation level.)

Table A1
Summary of model materials and element types.

Component	Element type	Material types	Density (kg/m^3)	Elastic modulus (GPa)	Poisson's ration	Reference
Cortical bone	2D-Shell	Viscoelasticity	1800–2000	12–20	0.3	Untaroiu et al. (2013)Anderson et al. (2005)
Cancellous bone	Hexahedral	Elastic plastic	861.5–1500	0.16–0.7	0.3	Schuster et al. (2000)
Knee ligaments	Hexahedral	Viscoelasticity	1200	3.75–4.3	0.3	(Mo et al., 2012; Mo et al., 2018) (Untaroiu et al., 2013)
Patellar ligament	Hexahedral	Elastic plastic	1320	0.225	0.4	Butler et al. (1986)
Meniscus	Hexahedral	Elastic	1500	0.25	0.3	Fithian et al. (1990)
Articular cartilage	2D-Shell	Elastic plastic	1800	0.045	0.4	Dakin et al. (2001)
Skin	2D-Shell	Elastic	920	1.17e-6	0.4	Al-Dirini et al. (2016)
Skeletal muscle	Hexahedral	Ogden	1060	5.6e-6	0.495	Myers et al. (1995); Myers et al. (1998)
Fat	Tetrahedron	Ogden	920	1.17e-6	0.4	Al-Dirini et al. (2016)
Tendon	1D Springs	Nonlinear elastic	–	a	–	Morrison et al. (2015)
Other tendons	1D Springs	Nonlinear	–	b	–	Maganaris and Paul (2010); Magnusson et al. (2010); Zajac (1989)

a. The resting length of Achilles tendon was set to 0.209 mm, and the stiffness was set as 201.8 N/mm according to Morrison et al. (2015).
b. Force-strain cruve for tibialis anterior tendon was extracted from Maganaris and Paul (1999). That for gastrocnemius tendon was extracted from Magunusson et al. (2008). Other tendon force-strain curves were scaled from tibialis anterior stress-strain curve based on tendon length, cross section area and 1.2 GPa Young's modulus (Zajac, 1989).

the previous study (Mo et al., 2018). Detailed material properties of the current model were illustrated in the Table A1.

As shown in Fig. A1, each muscle of the model is composed of three segments: tendon unit (TU), muscle passive unit (PU) and active contraction unit (CU). PU is surrounded by CU, which are represented by 3D hexagonal elements modeled with a hyperelastic material subject to the Ogden law (Eq. 1). The constitutive equation of the Ogden model is defined by a strain energy density function as follows:

$$W = \sum_{i=1}^{3}\sum_{j=1}^{n}\frac{\mu_j}{a_j}\left(\lambda_i^{a_j}-1\right)+\frac{1}{2}K(J-1)^2 \quad (1)$$

where μ_j and a_j are the model parameters to be determined, λ_i is the primary stretch, K is the bulk modulus, and J is the Jacobian. CU is modeled with a series of truss elements given by the improved Hill constitutive law. The active contraction force produced by the muscle was determined as follows,

$$F^{CE} = A(t)F_l(l)F_v(v)F_{\max} \quad (2)$$

where $A(t)$ is the muscle activation level, $F_l(l)$ is the normalized force–length curve, $F_v(v)$ is the force–velocity curve, and $F_{\max}$ is the maximum isometric force, which was obtained by multiplying the equivalent physiological cross-sectional area (PCSA) and the maximum stress $\sigma_{\max}$ of the target muscle. Then, the contraction force of the muscle was determined by the input signals between 0 and 1 of $A(t)$.

A 1.2. Validation of 3D active muscle with in-vivo volunteer experiments

The lower limb model has been validated according to the previous experiments results from isolated materials to sub-segments and finally the whole lower limb, especially considering its passive properties as shown in Table A2. Some detailed validation of the present lower limb has been reported in the previous studies (Mo et al., 2018; Wang, 2017). To improve its biofidelity in human locomotion analysis, we further validate its mechanical properties of the 3D active muscle with recent in-vivo volunteer experiments of Maïsetti et al. (2012).

Maïsetti et al. determined elongation mechanical properties of gastrocnemius medialis using supersonic shear imaging method during ankle dorsiflexion. Through ankle dorsiflexion, the torque–angle relationship, surface EMG activity and shear modulus of gastrocnemius medialis were measured. The normalized force-strain curves of gastrocnemius medialis were obtained and highly correlated with Hoang's model (Hoang et al., 2005). In the present validation, the normalized curve was used to evaluate our muscle model, while the shear modulus of the muscle model in relaxation was adjusted to 5.6 KPa according to the experimental measurements.

Based on Maïsetti et al. experiments (Maïsetti et al., 2012), the validation was implemented on the gastrocnemius medialis muscle, as shown in Fig. A2a. The proximal end of the gastrocnemius was constrained, and the distal end was applied with a constant velocity at 0.44 m/s along muscle fibers according to the experimental boundary condition. The simulation was carried out until 100 ms to ensure the elongation of muscle matching the

Table A2
Summary of lower limb model validation.

	Validation experiments	Experimental references	Parameters
Isolated Tissues	Quasi-static three-point bending of tibia, femur and fibula	(Kenedi, 1971) (Ehler and Lösche, 1970) (Asang, 1976) (Asang, 1976)	Force
	Quasi-static compression of femoral head	Keyak et al. (1998)	Force
	Dynamic three-point bending of tibia, femur and fibula	(Kerrigan et al., 2003) (Nyquist et al., 1985)	Force, Moment
Sub-segment	Dynamic foot axial impact	Kitagawa et al. (1998)	Force
	Dynamic pelvic lateral impact	Guillemot et al. (1997)	Force
	Dynamic knee-knee pad impact	Hayashi et al. (1996)	Force
	Dynamic knee-thigh impact	Rupp et al. (2002)	Force
Whole lower limb	Dynamic knee-thigh-hip impact	Rupp et al. (2002)	Force

experiments. The comparison of the simulation results to the experimental results was shown in Fig. A2b. A good correlation with the coefficient of determination R^2 equaling to 0.96 was noted. This further validated the biofidelity of the lower limb model especially concerning in vivo active muscle properties.

A 2. Details of joint angle calculation, control algorithm, neural delay and muscle activation dynamics

A 2.1. Knee joint angle calculation

The knee joint angle curve was the target of the present study. The knee joint real-time angle was calculated during the FE simulation by defining two vectors $\overrightarrow{U_1}$ and $\overrightarrow{U_2}$, as shown in Fig. A1. The reference nodes used for defining the two vectors were the proximal femoral node N_1 at the hip joint, the distal femoral node N_2, the proximal tibia node N_3, and the distal tibia node N_4. The knee joint angle was calculated from cross product of the two vectors in sagittal plane.

A 2.2. PID control algorithm

The error signal of the PID controller is the difference between the knee real-time angle and the target knee joint angle. The PID controller was established in the FE model with Ls-Dyna codes. It was used to calculate the control signal $u(t)$, which was then transferred to muscle activation levels based on muscle activation dynamics for lower extremity locomotion. In each time step, the muscle activation level was iteratively adjusted by the PID controller to minimize the signal error $e(t)$, namely minimize the knee joint angle difference between the simulation results and the experimental data. The formula for the PID controller was as follows:

$$e(t) = D(t) - y(t) \tag{1}$$

$$u(t) = k_p * yd(t) + k_i * \int_0^t yd(\tau)d\tau + k_d \frac{dyd(t)}{dt} \tag{2}$$

where $e(t)$ is the knee joint angle error signal, $yd(t)$is the real-time knee joint angle after neural delay, k_p,k_i and k_d are the proportional,

Table A3
List of acronyms appearance in the text.

Acronyms	Full name	Acronyms	Full name
PID	Proportion-Integration-Differentiation	Vasmed	Vastus medialis
CMC	Computed Muscle Control	Vaslat	Vastus lateralis
Semiten	Semitendinosus	Gasmed	Gastrocnemius medialis
Bicfemlh	Biceps femoris long head	Gaslat	Gastrocnemius lateralis
Rectfem	Rectus femoris	Tibant	Tibialis anterior

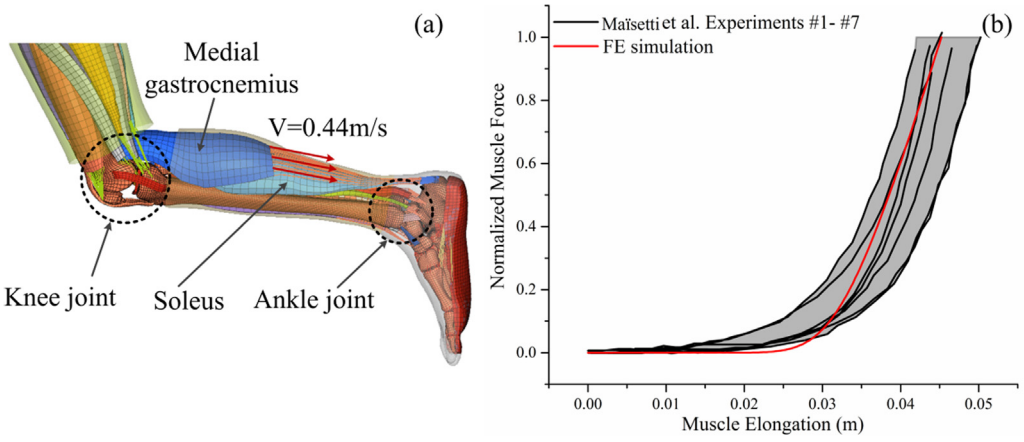

Fig. A2. Extension validation of the lower limb model muscle with in vivo experimental results.

integral, and differential gains of the PID controller, which were set as constant according to Andersson (2013) research.

A 2.3. CMC control algorithm

The CMC controller resulted from the musculoskeletal model in Opensim codes, which can be used to obtain muscle activation levels according to the desired kinematic trajectory of the human body. It has a proportion differentiation (PD) controller and a static optimization strategy. The PD controller calculates a series of expected acceleration $\ddot{q}^*$ to drive model trajectory q reach the experimental trajectory $q_{\exp}$ as follows (Thelen and Anderson, 2006):

$$\ddot{q}(t+T) = \ddot{q}_{\exp}(t+T) + k_v\left[\dot{q}_{\exp}(t) - \dot{q}(t)\right] + k_p\left[q_{\exp}(t) - q(t)\right] \quad (3)$$

where $\ddot{q}$ is the model acceleration, $\ddot{q}_{\exp}$ is the experimental acceleration, k_v and k_p are feedback control gains based on speed and position error, respectively. The static optimization method was used to minimize the joint load difference between the objective values and actuators. The chosen cost function in this study is as follows:

$$J = \sum_{i=1}^{n} x_i^2 + \sum_{j=1}^{n} w_j\left(\ddot{q}_j^* - \ddot{q}_j\right)^2 \quad (4)$$

where x is the actuator control, and w_j is the desired coefficient, $\ddot{q}_j^*$ is the expected acceleration, $\ddot{q}_j$ is the model acceleration.

A 2.4. Neural delay simulation

Since time is required for nerve signals to pass from the central nervous system to the muscle actuator, the inclusion of a neural delay simulates this process: receptors receive external stimulation signals, then the central nervous system makes neuromodulation, and finally, the actuator responds accordingly. The neural delay was set to 20 ms based on previous studies (Barrett et al., 2007). In the physical control model, a low-pass filter was often used to simulate signal delay. Therefore, in this study the phase delay of the first-order inertial link was used to achieve neural delay.

A 2.5. Muscle activation dynamics

Muscle activation dynamics were governed by the mechanisms initiated by the action potential at the neuromuscular joint. These mechanisms controlled the flux of potassium and sodium ions in and out of the muscle fiber membrane in response to impulses, the flux of potassium and sodium ions caused an action potential to propagate, while the flux of calcium ions leaded to the sliding motion of muscle filaments in the sarcomere (Marieb and Hoehn, 2010). Muscle activation dynamics contained two parts: generation of the action potential and generation the muscle activation levels. Therefore, Winters and Stark (1985) used low-pass filters to simulate the muscle activation dynamics mechanism. The first filter simulated the process of obtaining neural stimulation $Ne(t)$ from the muscle stimulation signal $u(t)$, which aimed to simulate the release process of potassium and sodium ions during action potential stimulation. The second filter was used to limit the muscle activation level range to obtain $A(t)$, which aimed to simulated the release of calcium ions from muscle fibers. Therefore, the formulas related to muscle activation dynamics are as follows:

$$T_{ne}\frac{dNe(t)}{dt} = \frac{u(t)}{M_{fe}} - Ne(t) \quad (5)$$

$$T_{na}\frac{dA(t)}{dt} = Ne(t) - A(t) \quad (6)$$

where T_{ne} and T_{na} are the time constants of the two low-pass filters: T_{ne} influences the output rate of the stimulus signal, and T_{na} refers to the response speed of the muscle, M_{fe} is the maximum moment of extension or flexion about the joint. Based on the previous studies, muscle activation levels are regulated in the region from 0% to 100%.

References

Al-Dirini, R.M.A., Reed, M.P., Hu, J., Thewlis, D., 2016. Development and validation of a high anatomical fidelity FE model for the buttock and thigh of a seated individual. Ann. Biomed. Eng. 44 (9), 1–12.

Anderson, A.E., Peters, C.L., Tuttle, B.D., Weiss, J.A., 2005. Subject-specific finite element model of the pelvis: development, validation and sensitivity studies. J. Biomech. Eng. 127 (3), 364–373.

Andersson, S., 2013. Active Muscle Control in Human Body Model Simulations - Implementation of a feedback control algorithm with standard keywords in LS-DYNA. MSc Thesis. Chalmers University of Technology; Gothenburg, Sweden.

Arnell, P., 1988. The biomechanics and motor control of human gait. Physiotherapy 74 (2), 94.

Arnold, E.M., Hamner, S.R., Seth, A., Millard, M., Delp, S.L., 2013. How muscle fiber lengths and velocities affect muscle force generation as humans walk and run at different speeds. J. Exp. Biol. 216 (11), 2150–2160.

Arnold, E.M., Martell, E.A., 2010. A model of the lower limb for analysis of human movement. Ann. Biomed. Eng. 38 (2), 269–279.

Asang, E., 1976. Experimental biomechanics of the human leg. A basis for interpreting typical skiing injury mechanisms. Orthop. Clin. North Am. 7 (1), 63–73.

Barrett, R.S., Besier, T.F., Lloyd, D.G., 2007. Individual muscle contributions to the swing phase of gait: an EMG-based forward dynamics modelling approach. Simul. Model. Pract. Theory 15 (9), 1146–1155.

Behr, M., Arnoux, P.J., Serre, T., Thollon, L., Brunet, C., 2006. Tonic finite element model of the lower limb. J. Biomech. Eng. 128 (2), 223–228.

Behr, M., Poumarat, G., Serre, T., Arnoux, P.J., Thollon, L., Brunet, C., 2010. Posture and muscular behaviour in emergency braking: an experimental approach. Accid. Anal. Prev. 42 (3), 797–801.

Bose, D., Crandall, J.R., 2008. Influence of active muscle contribution on the injury response of restrained car occupants. Ann. Adv. Automot. Med. 52, 61–72.

Brown, T.D., Shaw, D.T., 1985. Instantaneous in vitro contact stress distributions on the femoral condyles. J. Biomech. 18 (3), 227.

P. Budziszewski, K. Kędzior, J. Mordaka. Active controlled muscles in numerical model of human arm for movement in two degrees of freedom [C]//Bern, Switzerlan; 2008.

Butler, D.L., Kay, M.D., Stouffer, D.C., 1986. Comparison of material properties in fascicle-bone units from human patellar tendon and knee ligaments. J. Biomech. 19 (6), 425–432.

Chang, C.Y., Rupp, J.D., Kikuchi, N., Schneider, L.W., 2008. Development of a finite element model to study the effects of muscle forces on knee-thigh-hip injuries in frontal crashes. Stapp Car Crash J., 475–504

Chang, C.Y., Rupp, J.D., Reed, M.P., Hughes, R.E., Schneider, L.W., 2009. Predicting the effects of muscle activation on knee, thigh, and hip injuries in frontal crashes using a finite-element model with muscle forces from subject testing and musculoskeletal modeling. Stapp Car Crash J. 53, 291.

Chen, W.M., Lee Tlee, P.V., Lee, J.W., Lee, S.J., 2010. Effects of internal stress concentrations in plantar soft-tissue-A preliminary three-dimensional finite element analysis. Med. Eng. Phys. 32 (4), 324–331.

Chen, W.M., Park, J., Park, S.B., Shim, P.W., Lee, T., 2012. Role of gastrocnemius–soleus muscle in forefoot force transmission at heel rise — a 3D finite element analysis. J. Biomech. 45 (10), 1783–1789.

Chen, W.M., Lee, S.J., Lee, P.V., 2015. Plantar pressure relief under the metatarsal heads - therapeutic insole design using three-dimensional finite element model of the foot. J. Biomech. 48 (4), 659–665.

Dakin, G.J., Arbelaez, R.A., Molz, F.J., Alonso, J.E., Mann, K.A., Eberhardt, A.W., 2001. Elastic and viscoelastic properties of the human pubic symphysis joint: effects of lateral impact joint loading. J. Biomech. Eng. 123 (3), 218–226.

Dibb, A.T., Cox, C.A., Nightingale, R.W., Luck, J.F., Cutcliffe, H.C., Myers, B.S., Arbogast, K.B., Seacrist, T., Bass, C.R., 2013. Importance of muscle activations for biofidelic pediatric neck response in computational models. Traffic Inj. Prev. 14 (sup1), S116–S127.

Ehler, E., Lösche, H., 1970. Die menschliche tibia unter biegebelastung. Beitr. Orthop. 17 (5), 291–304.

Fithian, D.C., Kelly, M.A., Mow, V.C., 1990. Material properties and structure-function relationships in the menisci. Clin. Orthop. Relat. Res. 252 (252), 19–31.

Florio, C.S., 2018. Effectiveness of various isometric exercises at improving bone strength in cortical regions prone to distal tibial stress fractures. Int. J. Numer. Methods Biomed. Eng. 34 (6), e2976.

Fukubayashi, T., Kurosawa, H., 1980. The contact area and pressure distribution pattern of the knee. A study of normal and osteoarthrotic knee joints. Acta Orthop. Scand. 51 (6), 871–879.

Guillemot, H., Besnault, B., Robin, S., Got, C., Coz, J.Y.L., Lavaste, F., Lassau, J.P., 1997. Pelvic injuries in side impact collisions: a field accident analysis and dynamic tests on isolated pelvic bones. J. Passeng. Cars 106 (6), 3624–3633.

Guiotto, A., Sawacha, Z., Guarneri, G., Avogaro, A., Cobelli, C., 2014. 3D finite element model of the diabetic neuropathic foot: a gait analysis driven approach. J. Biomech. 47 (12), 3064–3071.

Halloran, J.P., Erdemir, A., 2011. Adaptive surrogate modeling for expedited estimation of nonlinear tissue properties through inverse finite element analysis. Ann. Biomed. Eng. 39 (9), 2388–2397.
Halloran, J.P., Marko, A., Ahmet, E., Bogert, A.J.V.D., 2010. Concurrent musculoskeletal dynamics and finite element analysis predicts altered gait patterns to reduce foot tissue loading. J. Biomech. 43 (14), 2810–2815.
Hayashi, S., Choi, H.Y., Levine, R.S., King, Y., 1996. Experimental and analytical study of knee fracture mechanisms in a frontal knee impact. J. Passen. Cars 105 (6), 1842–1852.
Hedenstierna, S., Brolin, P.H., 2008. Evaluation of a combination of continuum and truss finite elements in a model of passive and active muscle tissue. Comput. Methods Biomech. Biomed. Eng. 11 (6), 627–639.
Hoang, P.D., Gorman, R.B., Todd, G., Gandevia, S.C., Herbert, R.D., 2005. A new method for measuring passive length–tension properties of human gastrocnemius muscle in vivo. J. Biomech. 38 (6), 1333–1341.
Iwamoto, M., Nakahira, Y., Kimpara, H., Sugiyama, T., 2009. Development of a human FE model with 3-D geometry of muscles and lateral impact analysis for the arm with muscle activity. Sae Technical Papers.
Iwamoto, M., Nakahira, Y., Sugiyama, T., 2011. Investigation of pre-impact bracing effects for injury outcome using an active human FE model with 3D geometry of muscles. J. Jpn. Assoc. Certif. Orthop. 35, 147–154.
Iwamoto, M., Nakahira, Y., Kimpara, H., Sugiyama, T., Min, K., 2012. Development of a human body finite element model with multiple muscles and their controller for estimating occupant motions and impact responses in frontal crash situations. Stapp Car Crash J. 56, 231.
Jonkers, I., Stewart, C., Spaepen, A., 2003. The study of muscle action during single support and swing phase of gait: clinical relevance of forward simulation techniques. Gait Posture 17 (2), 97–105.
Kenedi, R.M., 1971. Strength of biological materials. J. Anat. 108 (Pt 3), 582.
Kerrigan, J.R., Bhalla, K.S., Madeley, N.J., Funk, J.R., Bose, D., Crandall, J.R., 2003. Experiments for establishing pedestrian-impact lower limb injury criteria. SAE Tech. Paper. 2003–01-0895.
Keyak, J.H., Rossi, S.A., Jones, K.A., Skinner, H.B., 1998. Prediction of femoral fracture load using automated finite element modeling. J. Biomech. 31 (2), 125–133.
Kitagawa, Y., Ichikawa, H., King, A.I., Levine, R.S., 1998. A severe ankle and foot injury in frontal crashes and its mechanism. J. Passen. Cars 107 (6), 2649–2660.
Lenhart, R.L., Kaiser, J., Smith, C.R., Thelen, D.G., 2015. Prediction and validation of load-dependent behavior of the tibiofemoral and patellofemoral joints during movement. Ann. Biomed. Eng. 43 (11), 2675–2685.
Lin, Y., Walter, J.P., Banks, S.A., Pandy, M.G., Fregly, B.J., 2010. Simultaneous prediction of muscle and contact forces in the knee during gait. J. Biomech. 43 (5), 945–952.
Maganaris, C.N., Paul, J.P., 1999. In vivo human tendon mechanical properties. J. Physiol. 521 (1), 307–313.
Maganaris, C.N., Paul, J.P., 2010. In vivo human tendon mechanical properties. J. Physiol. 521 (1), 307–313.
Magnusson, S.P., Narici, M.V., Maganaris, C.N., Michael, K., 2008. Human tendon behaviour and adaptation, in vivo. J. Physiol. 586 (1), 71–81.
Magnusson, S.P., Narici, M.V., Maganaris, C.N., Michael, K., 2010. Human tendon behaviour and adaptation, in vivo. J. Physiol. 586 (1), 71–81.
Maïsetti, O., Hug, F., Bouillard, K., Nordez, A., 2012. Characterization of passive elastic properties of the human medial gastrocnemius muscle belly using supersonic shear imaging. J. Biomech. 45 (6), 978–984.
Marieb, E.N., Hoehn, K., 2010. Human Anatomy and Physiology 8th issue [Z]. Pearson Benjamin Cummings, San Francisco.
Mo, F., Arnoux, P.J., Cesari, D., Masson, C., 2012. The failure modelling of knee ligaments in the finite element model. Int. J. Crashworth. 17 (6), 630–636.
Mo, F., Li, F., Behr, M., Xiao, Z., Zhang, G., Du, X., 2018. A lower limb-pelvis finite element model with 3D active muscles. Ann. Biomed. Eng. 46 (1), 86–96.
Morrison, S.M., Dick, T.J., Wakeling, J.M., 2015. Structural and mechanical properties of the human Achilles tendon: sex and strength effects. J. Biomech. 48 (12), 3530–3533.
Myers, B.S., Ee, C.A.V., Camacho, D.L.A., Woolley, C.T., Best, T.M., 1995. On the structural and material properties of mammalian skeletal muscle and its relevance to human cervical impact dynamics. SAE Tech. Paper 952723.
Myers, B.S., Woolley, C.T., Slotter, T.L., Garrett, W.E., Best, T.M., 1998. The influence of strain rate on the passive and stimulated engineering stress–large strain behavior of the rabbit tibialis anterior muscle. J. Biomech. Eng. 120 (1), 126–132.
Nyquist, G.W., Cheng, R., El-Bohy, A.A.R., King, A.I., 1985. Tibia bending: strength and response. SAE Tech. Paper, 851728.
Osth, J., Brolin, K., Happee, R., 2012. Active muscle response using feedback control of a finite element human arm model. Comput. Methods Biomech. Biomed. Eng. 15 (4), 347–361.
Osth, J., Brolin, K., Carlsson, S., Wismans, J., Davidsson, J., 2012. The occupant response to autonomous braking: a modeling approach that accounts for active musculature. J. Crash Prev. Inj. Contr. 13 (3), 265–277.
Osth, J., Eliasson, E., Happee, R., Brolin, K., 2014. A method to model anticipatory postural control in driver braking events. Gait Posture 40 (4), 664–669.
Phillips, A.T.M., Villette, C.C., Modenese, L., 2015. Femoral bone mesoscale structural architecture prediction using musculoskeletal and finite element modelling. Int. Biomech. 2 (1), 43–61.
Rupp, J.D., Reed, M.P., Van Ee, C.A., Kuppa, S., Wang, S.C., Goulet, J.A., Schneider, L.W., 2002. The tolerance of the human hip to dynamic knee loading. Stapp Car Crash J. 46 (46), 211–228.
Salin, D., Arnoux, P.J., Kayvantash, K., Behr, M., 2016. Implementation of reflex loops in a biomechanical finite element model. Comput. Methods Biomech. Biomed. Eng. 19 (14), 1578–1582.
Sangbaek, P., Seungju, L., Jeongro, Y., Soo-Won, C., 2019. Finite element analysis of knee and ankle joint during gait based on motion analysis. Med. Eng. Phys. 63, 33–41.
Scarton, A., Guiotto, A., Malaquias, T., Spolaor, F., Sinigaglia, G., Cobelli, C., Jonkers, I., Sawacha, Z., 2018. A methodological framework for detecting ulcers' risk in diabetic foot subjects by combining gait analysis, a new musculoskeletal foot model and a foot finite element model. Gait Posture 60, 279.
Schuster, P.J., Chou, C.C., Prasad, P., Jayaraman, G., 2000. Development and validation of a pedestrian lower limb non-linear 3-d finite element model. Stapp Car Crash J. 44, 315.
Shirazi, R., Shirazi-Adl, A., Hurtig, M., 2008. Role of cartilage collagen fibrils networks in knee joint biomechanics under compression. J. Biomech. 41 (16), 3340–3348.
Stops, A., Wilcox, R., Jin, Z.M., 2012. Computational modelling of the natural hip: a review of finite element and multibody simulations. Comput. Methods Biomech. Biomed. Eng. 15 (9), 963–979.
Thelen, D.G., Anderson, F.C., 2006. Using computed muscle control to generate forward dynamic simulations of human walking from experimental data. J. Biomech. 39 (6), 1107–1115.
Thelen, D.G., Kwang, W.C., Schmitz, A.M., 2014. Co-simulation of neuromuscular dynamics and knee mechanics during human walking. J. Biomech. Eng. 136 (2), 21033.
Untaroiu, Costin D, Yue, Neng, Shin, Jaeho, 2013. A finite element model of the lower limb for simulating automotive; impacts. Ann. Biomed. Eng. 41 (3), 513–526.
Valente, G., Crimi, G., Vanella, N., Schileo, E., Taddei, F., Valente, G., Crimi, G., Vanella, N., Schileo, E., Taddei, F., 2017. NMSBUILDER: freeware to create subject-specific musculoskeletal models for OpenSim. Comput. Methods Programs Biomed. 152. S394383169X.
Wang, Y., Cao, L., Bai, Z., Reed, M.P., Rupp, J.D., Hoff, C.N., Hu, J., 2016. A parametric ribcage geometry model accounting for variations among the adult population. J. Biomech. 49 (13), 2791–2798.
Wang X S. 2017. Research on driver KTH damage in frontal collision based on 3D active muscle lower limb model [D]. MSc Thesis, Hunan University; Changsha, China.
Winters, J.M., Stark, L., 1985. Analysis of fundamental human movement patterns through the use of in-depth antagonistic muscle models. IEEE Trans. Biomed. Eng. 32 (10), 826–839.
Zajac, F.E., 1989. Muscle and tendon: properties, models, scaling, and application to biomechanics and motor control. Crit Rev Biomed Eng 17 (4), 359–411.
Zhihui, Q., Lei, R., Yun, D., Hutchinson, J.R., Luquan, R., 2013. A dynamic finite element analysis of human foot complex in the sagittal plane during level walking. Plos One 8 (11), e79424.